Int. J. Heat Mass Transfer. Vol. 33, No. 1, pp. 91–103, 1990
Printed in Great Britain

0017–9310/90 $3.00 + 0.00

Contact angle effects on boiling incipience of highly-wetting liquids

W. TONG, A. BAR-COHEN, T. W. SIMON and S. M. YOU
Department of Mechanical Engineering, University of Minnesota, Minneapolis, MN 55455, U.S.A.

(*Received* 12 *October* 1988 *and in final form* 28 *April* 1989)

Abstract—The difficulty in predicting the boiling incipience of highly-wetting liquids has slowed the application of immersion cooling technology in the electronics industry. The present effort sheds new light on this phenomenon by examining the influence of the dynamic solid/liquid contact angle and contact angle hysteresis on the incipience superheat. The results suggest that variations in contact angle, induced by changes in the direction and magnitude of the liquid/vapor interface velocity, can substantially affect the formation of bubble embryos and may well explain the wide experimental scatter in incipience superheat values reported for highly-wetting liquids.

INTRODUCTION

IN RECENT years, interest has grown in the use of immersion cooling techniques for both advanced electronic devices and supercomputer systems. The advantages of the high efficiency of such techniques have been recognized and immersion cooling has become the subject of a considerable amount of research by many companies and universities. One important reason for such attention is the rapid development of very large and ultra-large scale integration (VLSI and ULSI) microelectronic devices. With today's technology, it is possible to fabricate ICs with nearly 1 million components per chip. Chip density is expected to reach 10 million components by 1990 and a billion components or more by the end of this century [1]! As a result, chip heat flux could reach as high as 125 W cm^{-2} in the early 1990s, which is nearly four times the present level [2].

It is this challenge that has focused special attention on the use of flow and pool boiling, as well as impinging jet boiling, of dielectric liquids for thermal control of electronic components. The perfluorinated fluids, represented by the Fluorinerts or 'FC' series of the 3M Company (St. Paul, Minnesota), and the chlorofluorocarbons, represented by the Freon refrigerant series of the Du Pont Company (Wilmington, Delaware), are widely used dielectric fluids. Both fluid groups possess a relatively low surface tension and have been found to display highly-wetting behavior on most known surfaces.

While boiling heat transfer encompasses a variety of thermal transport phenomena, it is the highly efficient nucleate boiling regime that is of primary interest for thermal control. This regime lies between boiling incipience, associated with a steady release of vapor bubbles from distinct nucleation sites, and the critical heat flux, associated with vapor blanketing of the heated surface.

The effect of surface conditions on nucleate boiling has long been the subject of extensive studies. Corty and Foust [3] may well have been the first to relate the presence of vapor bubbles trapped in microcavities on the surface to nucleate boiling. Bankoff [4] suggested that vapor and/or air could be trapped in wedge-shaped grooves if the contact angle of the liquid on the solid surface is greater than the wedge angle; otherwise, such grooves would be flooded by the liquid. A similar condition would be required to assure that conical cavities on the surface contain embryonic vapor/air bubbles. These early investigators viewed the vapor/air filled cavities as potential nucleation sites, which could be 'activated', i.e. induced to produce a steady stream of vapor bubbles, at an appropriate value of surface superheat.

Griffith and Wallis [5] concluded that the contact angle is important in bubble nucleation primarily through its effect on the stability of the bubble within the cavity and that for a contact angle which lies between the half-conical angle of the cavity, ϕ, and 90° the superheat required to activate a nucleation site will be determined by the cavity-mouth radius. In 1962, Hsu [6] proposed a method for determining the range of active nucleation sites as a function of wall temperature or heat flux. Hsu's model revealed that the maximum and minimum sizes of active cavities (implicitly limited to cavities with a large depth-to-radius ratio) are functions of subcooling, system pressure, physical properties, and the thickness of the superheated liquid layer. By assuming that a bubble is departing from a conical cavity with a given radius and cone angle, Lorenz [7] analyzed the vapor trapping process following bubble departure and used geometric relations to determine the radius of a trapped bubble embryo. He concluded that the ratio of the embryo radius to the cavity radius is a function of a static equilibrium contact angle, β_s, and a cone

NOMENCLATURE

D_b	departure diameter [m]
P	pressure [N m^{-2}]
P^*	pressure inside bubble [N m^{-2}]
q''	heat flux [W m^{-2}]
R	bubble radius [m]
R_0	cavity radius [m]
T	temperature [K]
T_L	superheat limit [K]
ΔT_s	wall superheat on boiling curves [K]
$(\Delta T_s)_i$	incipience superheat [K]
V	volume [m^3].

Greek symbols

β	contact angle
β_d	dynamic contact angle
$\beta_{d,A}$	dynamic advancing contact angle
$\beta_{d,R}$	dynamic receding contact angle
β_s	static equilibrium contact angle
$\beta_{s,A}$	static advancing contact angle
$\beta_{s,R}$	static receding contact angle
2ϕ	conical angle
ρ	density [kg m^{-3}]
σ	surface tension [N m^{-1}] or surface energy [J m^{-2}].

Subscripts

C	critical property
g	gas
ℓ	liquid
s	saturated property
v	vapor
w	wall
0	cavity.

angle, 2ϕ. A detailed review of the gas trapping processes was given by Cole [8]. In succeeding paragraphs, the emphasis will be placed on the influence of the dynamic contact angle on the vapor/air trapping process as related to heterogeneous nucleation of boiling and the influence of contact angle hysteresis on the bubble growth process.

CONTACT ANGLE AND ITS HYSTERESIS

The contact angle between a liquid and a solid surface is one of the most important factors in boiling heat transfer since it characterizes the wettability of a certain solid surface by a specific liquid. Many parameters, such as the volume of trapped vapor/air in a cavity, critical bubble radius, incipience superheat and the superheat excursion at the onset of nucleate boiling, are strongly influenced by surface wettability. Despite recent interest and the use of more advanced techniques for measuring contact angles [9], the complexity of the wetting phenomenon has, thus far, stymied the research community and there is no general formula for predicting the contact angle.

The complexity results from both solid surface effects and liquid characteristics. Real solid surfaces are usually heterogeneous, anisotropic, rough, and are affected by adsorption and oxidation. Liquids may experience chemical reactions at the solid–liquid interfaces and may possess and/or develop impurities which tend to concentrate at the interfaces.

According to the state of motion of the liquid–solid–gas boundary (three phase contact line), the contact angle can be classified as a static contact angle or dynamic contact angle. Experimental work has shown that dynamic contact angles are dependent on the velocity of the interface at the contact line. Three relations for dynamic contact angle–velocity behavior have been proposed in different velocity ranges as the liquid–vapor/air interface moves toward the vapor/air region [10]. In the lowest velocity range ($\lesssim 1$ mm min^{-1} for water), the dynamic contact angle, β_d, has been found to equal the static contact angle, β_s, but at higher velocities, $\beta_d > \beta_s$. This indicates that at high interface velocities even for highly-wetting liquids, the dynamic contact angle may be sufficiently large to trap gas and form bubble embryos in surface cavities. Experimental studies have shown that the magnitude of the static equilibrium contact angle has no effect on the relationship between β_d and velocity [10]. For instance, for a stainless steel–hexadecane system, the static equilibrium contact angle is observed to be near zero, but the dynamic contact angle is as high as 75° when the liquid velocity is about 9.7 cm s^{-1}. However, at the same velocity, the dynamic contact angle for a Teflon–octane system ($\beta_s = 26°$) only reaches 48° [10]. Johnson and Dettre [11] reported that the effect of interface velocity on contact angle is negligible or very small on homogeneous surfaces but becomes significant on heterogeneous surfaces. If unspecified, 'contact angle' usually refers to the static equilibrium angle since it is usually measured under static conditions.

The contact angles of FC and Freon refrigerants are very small (Table 1), approaching zero on surfaces of polished copper and stainless steel [10, 13, 15]. The FC series liquids are derived from common organic compounds by replacement of all carbon-bound hydrogen atoms with fluorine atoms. The exposed C_nF_{2n+2} ($n = 5$–10) groups of the liquid molecules make the Fluorinert (FC series) liquids extremely nonpolar and lead to a low surface tension and the associated high wettability and low contact angle [18].

Measurements of contact angles have shown the existence of a contact angle hysteresis. Static contact angle hysteresis is shown in Fig. 1 [11]. In the experiment illustrated in this figure, a liquid was supplied

Table 1. Observed values of static contact angle for some highly-wetting liquids

Liquid	Contact angle (deg)	Solid surface	Reference
Freon TF	0	Stainless steel	[10]
	0	Titanium	[10]
	0	Nylon	[10]
R-113	1–4	Stainless steel†	[12]
	2–4	Teflon†	[12]
	2–5	Stainless steel‡	[12]
	2–4	Teflon‡	[12]
R-113	~0	Polished copper	[13]
R-113	<5	Copper	[14]
R-11	<5	Copper	[14]
FC-72	~0	Stainless steel	[15]
FC-72	<1	Stainless steel	[16]
FC-77	~0.75§	Silicon	[17]
FC-84	~0.85§	Silicon	[17]

† Covered by R-113 vapor.
‡ Covered by air.
§ Calculated from the measured wetting film thickness data.

through a tiny hole in the surface so that a drop of the liquid was formed and forced to grow. During the process, a maximum contact angle, $\beta_{s,A}$, was observed. The value of $\beta_{s,A}$ is called the 'static advancing contact angle'. Also, if a liquid is withdrawn from the hole, a minimum contact angle, $\beta_{s,R}$, is observed. The value of $\beta_{s,R}$ is called the 'static receding contact angle'. Obviously, β_s must always lie between $\beta_{s,A}$ and $\beta_{s,R}$ [11]. The definitions of dynamic advancing and receding contact angles can be made in a similar way as follows. As shown in Fig. 2, a dynamic advancing contact angle (maximum value), $\beta_{d,A}$, is reached when the liquid–vapor/air interface moves toward the vapor/air region at a certain velocity within a parallel channel and a dynamic receding contact angle (minimum value), $\beta_{d,R}$, is obtained when the liquid–vapor/air interface moves toward the liquid region. The differences between the two angles, i.e. $\beta_{s,A}-\beta_{s,R}$ and $\beta_{d,A}-\beta_{d,R}$, are defined as the static and dynamic contact angle hystereses, respectively. If not otherwise noted, contact angle hysteresis in this paper will refer to the static configuration.

Based on the above analysis and the discussion in ref. [19], the following relationship can be observed:

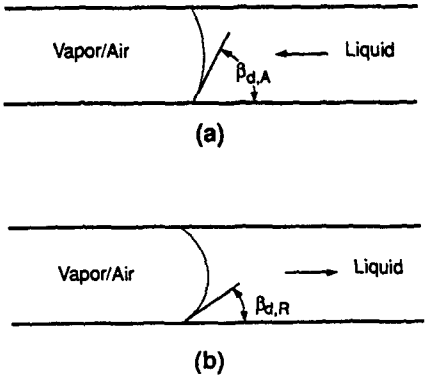

FIG. 2. Dynamic contact angle hysteresis: (a) dynamic advancing; (b) dynamic receding contact angle.

$$\beta_{d,A} > \beta_{s,A} \geq \beta_s \geq \beta_{s,R} > \beta_{d,R}. \quad (1)$$

The dynamic contact angle, β_d, is in the range

$$\beta_{d,A} \geq \beta_d \geq \beta_s \quad (2a)$$

when the interface moves toward the vapor/air region; and in the range

$$\beta_s \geq \beta_d \geq \beta_{d,R} \quad (2b)$$

when the interface moves toward the liquid region. In the present study, both cases will be considered.

Contact angle hysteresis is related to the degree of heterogeneity and roughness of solid surfaces [11, 20]. By comparing the effects of roughness with heterogeneity, Johnson and Dettre [11] found that roughness can cause hysteresis when the 'rugosities' are larger than about 0.5 μm. This value is often exceeded on polished commercial surfaces (rugosities are about 1 μm) but 'super finishing' generally results in lower values (0.05–0.5 μm).

BOILING INCIPIENCE

Conventional models for heterogeneous nucleate boiling relate boiling incipience to the surface superheat at which unrestrained bubble growth occurs [6, 21, 22]. More recently, based on Mizukami's [23] earlier development, Thormählen [24] proposed a boiling incipience criterion based on the stability of bubble growth. For $\beta_s < \phi + \pi/2$, when both the vol-

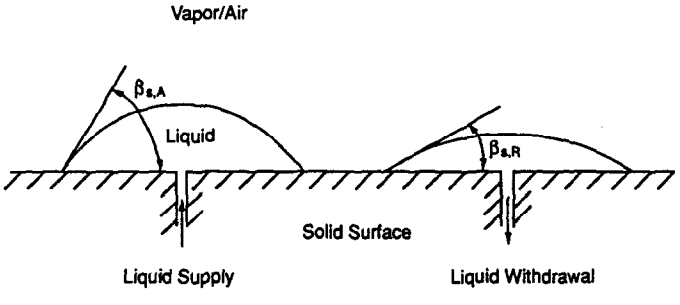

FIG. 1. Static advancing and receding contact angle [11].

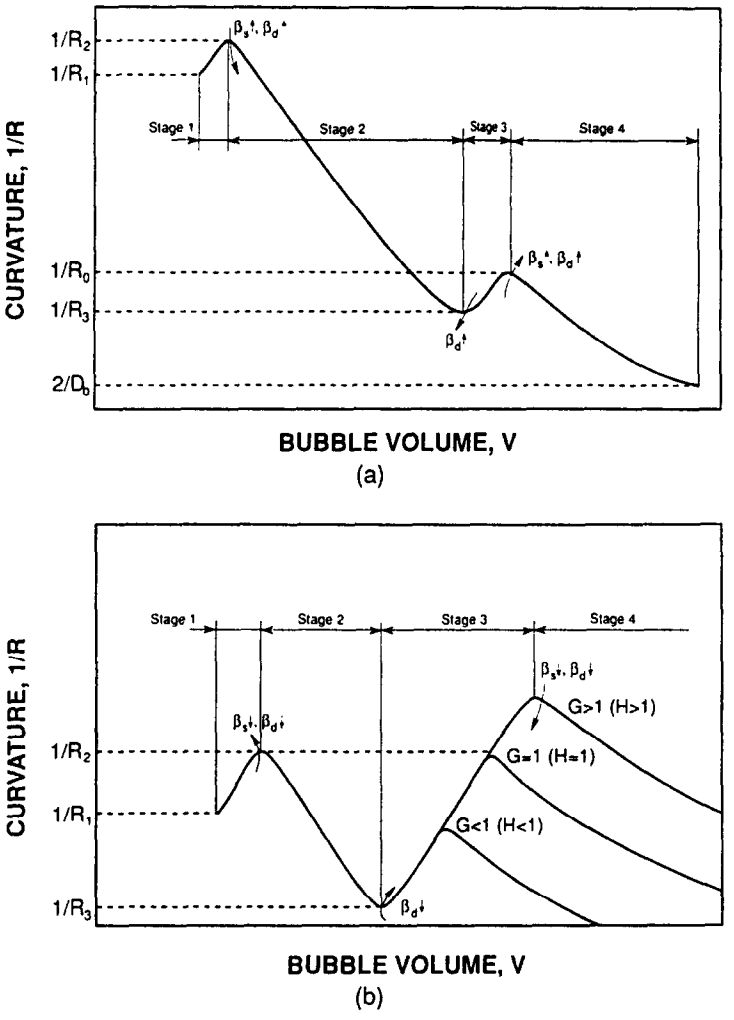

FIG. 3. Interface curvature vs bubble volume during bubble growth: (a) highly-wetting liquids, (b) moderately-wetting and poorly-wetting liquids (but $\beta_s < \phi + \pi/2$).

ume and radius of curvature of a bubble are increasing, the bubble will spontaneously grow, if

$$\frac{d}{dV}\left(\frac{1}{R}\right) < 0. \tag{3}$$

During bubble growth, the inverse bubble radius varies in a complex manner with bubble volume. As shown schematically in Figs. 3 and 4, this variation is seen to pass through four distinct stages:

(a) contact angle readjustment (due to contact angle hysteresis) (Fig. 4(a));
(b) in-cavity growth (Fig. 4(b));
(c) growth at the cavity mouth (Fig. 4(c));
(d) growth on the outer surface (Fig. 4(d)) and bubble departure.

Since these four stages have alternating slopes in the coordinates of inverse bubble radius, $(1/R)$, vs the bubble volume, V, the locus of the bubble growth process generally displays two 'humps' (Fig. 3). The bubble is on the verge of unrestrained growth when the slope turns from positive to negative with increasing bubble volume.

Under steady-state conditions, the pressure in the bubble and, hence, the wall superheat can be expected to vary directly with the inverse bubble radius [25]. Consequently, as first suggested by Han and Griffith [22], the superheat needed to insure bubble growth is determined by the largest value of the inverse bubble radius which meets the criterion of equation (3). Boiling incipience can thus be defined to occur at the highest peak of the two 'humps' where the maximum value of the reciprocal radius, $1/R$, is found. The wall superheat associated with this critical radius is then the incipience superheat, $(\Delta T_s)_i$, required for boiling initiation.

HETEROGENEOUS NUCLEATION ANALYSIS

The term 'heterogeneous nucleation' has been applied to those events where embryonic vapor/gas nuclei form in surface cavities and grow on heated surfaces. In contrast with this mode, homogeneous

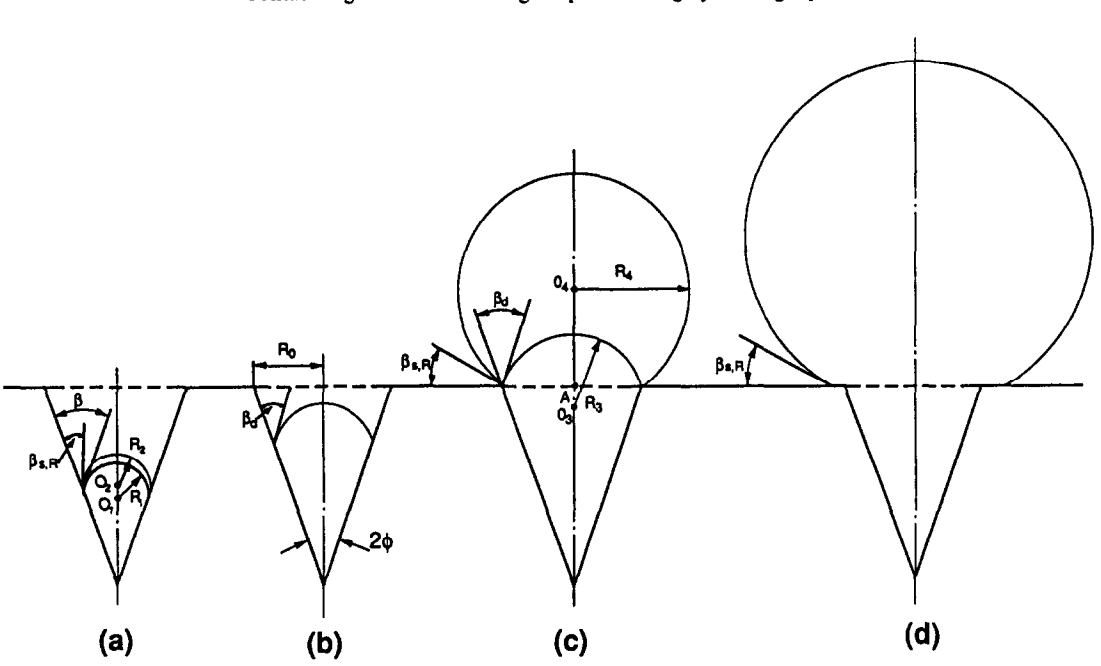

FIG. 4. Bubble growth stages: (a) contact angle readjustment; (b) in-cavity growth; (c) growth on the cavity mouth and contact angle readjustment; (d) growth on outer surface.

nucleation occurs when vapor nuclei, formed from a few 'energetic' molecules, grow within a superheated liquid. A criterion for dividing heterogeneous and homogeneous nucleation is given as a superheat limit, T_L. Studies [26–28] have shown that for totally degassed liquids with no nuclei within cavities on wetted surfaces (walls or particles within the fluid), no vaporization occurs below this superheat limit. By contrast, when the liquid reaches this superheat limit, which is normally much higher than the saturation temperature, homogeneous nucleation takes place with an extremely rapid bulk liquid-to-gas phase transformation.

In this section only heterogeneous boiling is addressed. The effects of dynamic contact angle on the vapor/gas trapping process are analyzed and a modification to the Lorenz [7] model is presented.

Vapor/air trapping process

Consider an idealized conical cavity with cone angle, 2ϕ, and mouth radius, R_0 (Fig. 5). A liquid flows into the cavity while keeping a constant dynamic contact angle, β_d (where $\beta_{d,A} \geqslant \beta_d \geqslant \beta_s$), with the cavity wall. Applying the dynamic contact angle idea to the trapping condition of Bankoff [4], heterogeneous nucleation of a bubble occurs as a result of the trapping vapor and non-condensable gas if

$$\beta_d > 2\phi. \tag{4}$$

For small contact angle liquids, the resulting bubble embryo, composed of trapped gas and vapor, establishes a convex interface as seen by the liquid phase (Fig. 5(b)). Thus, the total pressure inside the bubble embryo exceeds the system pressure. Following Lorenz [7], it may be assumed that the interface remains planar during the gas trapping process (Fig. 5(a)) and that no air diffusion, vapor condensation or liquid vaporization occurs during this process or from the bubble embryo after trapping. The present analysis differs from that of Lorenz in relating the vapor trapping volume to the dynamic contact angle, β_d, rather than β_s.

The volume of the trapped vapor/air (Fig. 5(a)) in the cavity equals the volume of an obliquely truncated right circular cone. This volume can be found by determining the area of a vertical slice through the trapped volume and integrating from $-x_0$ to $+x_0$. The result of this series of operations is given by

$$V_g(\beta_d, \phi, R_0) = \frac{4}{\tan\phi}\int_0^{x_0}\left\{\left(\frac{A}{A+1}\right)^2 \times R_0\sqrt{\left(R_0^2 - x^2\frac{A+1}{A-1}\right)} - \tfrac{1}{4}\left[y_2\sqrt{(x^2+y_2^2)} - y_1\sqrt{(x^2+y_1^2)} + x^2\ln\frac{y_2+\sqrt{(x^2+y_2^2)}}{y_1+\sqrt{(x^2+y_1^2)}}\right]\right\}dx \tag{5}$$

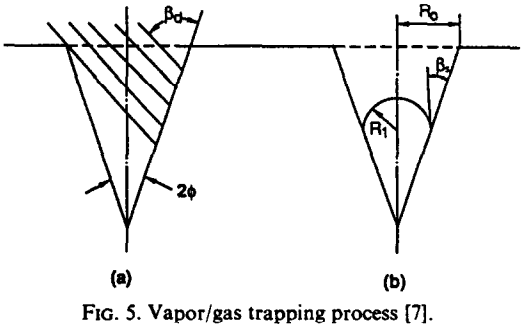

FIG. 5. Vapor/gas trapping process [7].

where

$$A = \frac{\tan(\beta_d - \phi)}{\tan\phi}$$

$$x_0 = R_0\left(1 - \frac{1}{A}\right)$$

and

$$y_1 = \frac{-R_0 - A\sqrt{\left(R_0^2 - x^2\frac{A+1}{A-1}\right)}}{A+1}$$

$$y_2 = \frac{-R_0 + A\sqrt{\left(R_0^2 - x^2\frac{A+1}{A-1}\right)}}{A+1}.$$

Lorenz provided an expression for the trapped gas volume in terms of the static contact angle, β_s, as

$$V_g(\beta_s, \phi, R_0) = \frac{\pi R_0^3}{3}\frac{\sin(\beta_s - 2\phi)\left[\frac{\tan\phi}{\tan(\beta_s - \phi)} - 1\right]^2}{\sin\phi\sin(\beta_s - \phi)\left[1 - \frac{\tan^2\phi}{\tan^2(\beta_s - \phi)}\right]^{3/2}}. \quad (6)$$

Substitution of β_d for β_s in equation (6) yields V_g values nearly equal to those calculated via equation (5).

Following Lorenz, the radius of curvature of the liquid/vapor interface for the embryonic bubble can be related to the trapped vapor/air volume, according to

$$R_1 = \left\{\frac{1}{\pi}\frac{3V_g(\beta_d, \phi, R_0)}{\frac{\cos^3(\beta_s - \phi)}{\tan\phi} + [2 - 3\sin(\beta_s - \phi) + \sin^3(\beta_s - \phi)]}\right\}^{1/3} \quad (7)$$

Consequently, the embryonic bubble radius, R_1, is seen to be dependent on the cavity radius, R_0, the cavity half angle, ϕ, the dynamic contact angle, β_d, and the static equilibrium contact angle, β_s, or

$$\frac{R_1}{R_0} = F(\beta_d, \beta_s, \phi). \quad (8)$$

In order to clarify the influence of the dynamic contact angle on the vapor/air trapping process, the ratio of the bubble radius to the cavity radius, R_1/R_0, is plotted in Figs. 6(a)–(c) vs the difference between the dynamic contact angle and the static equilibrium contact angle, $\beta_d - \beta_s$, for $\beta_s = 2°$, 30° and 50°, respectively. From these figures it may be observed that when the static equilibrium contact angle is fixed and the dynamic contact angle increases (i.e. $\beta_d - \beta_s$ increases), R_1/R_0 increases. However, for highly-wetting liquids (e.g. $\beta_s = 2°$), the R_1/R_0 values always lie below unity; for moderately-wetting liquids, R_1/R_0 can be greater than 1.0 in the larger dynamic contact angle region, especially for small cavity angles (Figs. 6(b) and (c)). It also can be seen that for highly-wetting liquids, the effect of dynamic contact angle on R_1/R_0 is significant only when the dynamic contact

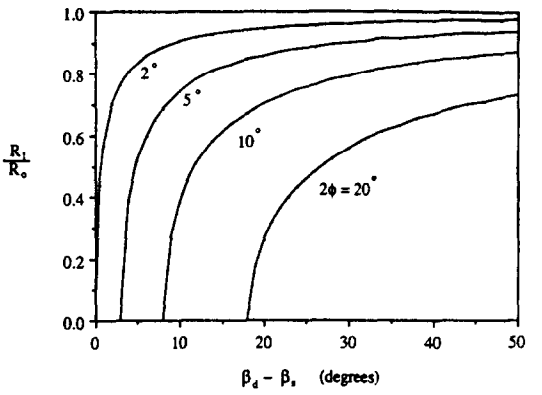

FIG. 6(a). The effect of dynamic contact angle on the ratio of bubble embryo radius to cavity radius for highly-wetting liquids ($\beta_s = 2°$).

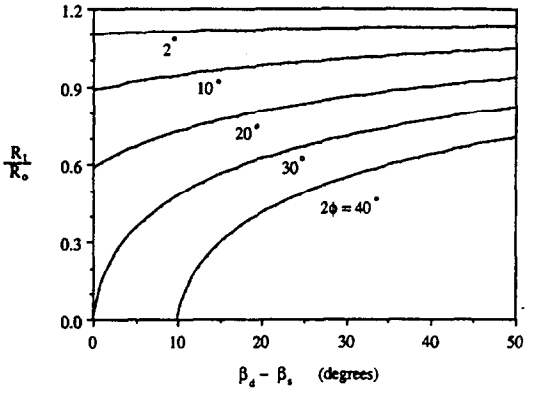

FIG. 6(b). The effect of dynamic contact angle on the ratio of bubble embryo radius to cavity radius for the liquids with $\beta_s = 30°$.

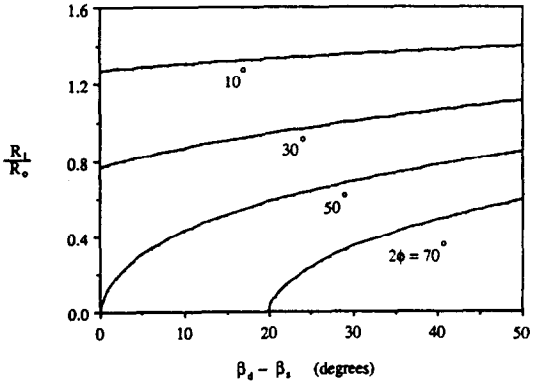

FIG. 6(c). The effect of dynamic contact angle on the ratio of bubble embryo radius to cavity radius for the liquids with $\beta_s = 50°$.

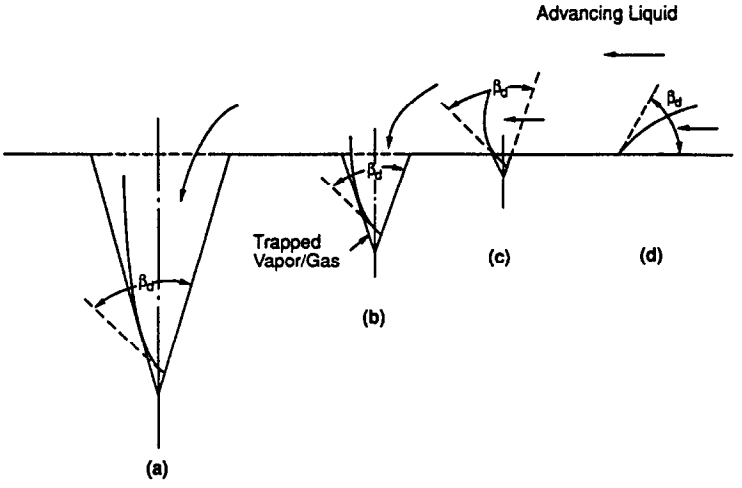

FIG. 7. The effect of cavity sizes on trapped vapor/gas volume.

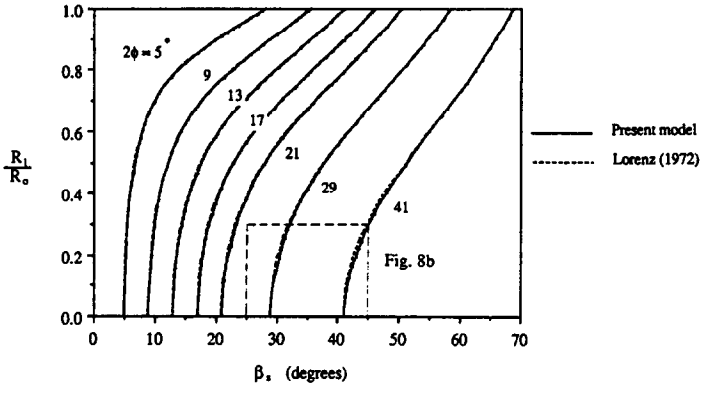

FIG. 8(a). Comparison of the present model (assuming $\beta_d = \beta_s$) and Lorenz's model [7]—for $0 < \beta_s < 70°$.

angle is small and the effect becomes negligible when the dynamic contact angle is large.

As previously noted by Lorenz [7], Bar-Cohen and Simon [29], Marsh and Mudawwar [16] and by reference to Fig. 6(a), the bubble critical radius is smaller than the radius of the mouth of the cavity for highly-wetting liquids. For moderately-wetting liquids, such as water, the bubble critical radius could equal the cavity radius under the conditions of small cavity angles and large dynamic contact angles (Figs. 6(b) and (c)).

When R_0 is large, perhaps in the hundreds of micrometer range for water and tens of micrometer range for highly-wetting liquids, the liquid/gas interface during the trapping process may depart from planarity and, if so, the above equations do not strictly apply (see Figs. 7(a) and (b)). Consequently, when R_0 is very large, the volume of the vapor/gas trapped by the curved interface can become independent of R_0. In the present study, however, R_0 is restricted to relatively small values.

Modified Lorenz correlation

A comparison of R_l/R_0 values computed from equation (7) but with (a) V_g computed from equation (5) (assuming $\beta_d = \beta_s$) and (b) V_g computed from the Lorenz expression (equation (6)) is shown in Figs. 8(a) and (b). The relatively modest differences suggest that the far simpler algebraic form of the Lorenz vapor trapping equation can be used as the basis for an R_l/R_0 relation involving both the static and dynamic contact angles. Proceeding in this manner, the radius

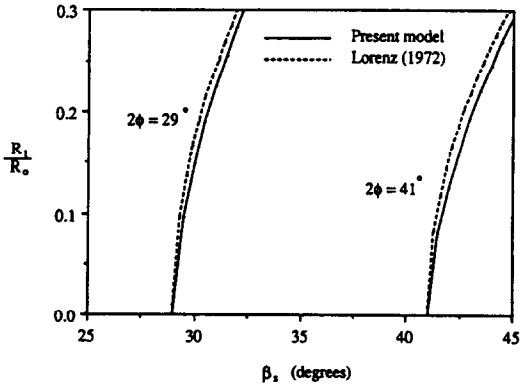

FIG. 8(b). Comparison of the present model (assuming $\beta_d = \beta_s$) and Lorenz's model—expanded view for $25° < \beta_s < 45°$.

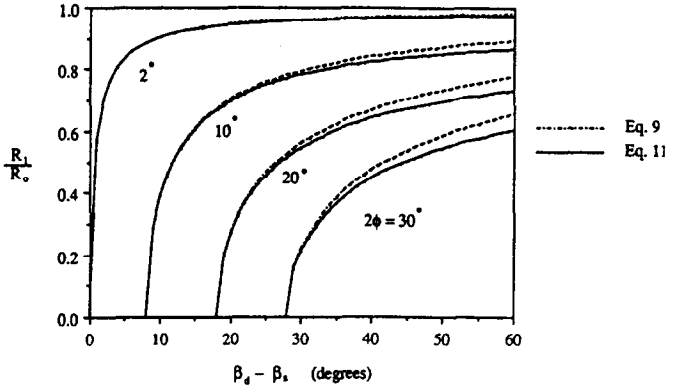

FIG. 9. Comparison of equations (9) and (11) for highly-wetting liquids ($\beta_s = 2°$) under different dynamic contact angles.

ratio is found to equal

$$\frac{R_1}{R_0} = \left\{ \frac{\dfrac{\sin(\beta_d - 2\phi)}{\sin(\beta_d - \phi)\sin\phi}}{\dfrac{\cos^3(\beta_s - \phi)}{\tan\phi} + [2 - 3\sin(\beta_s - \phi) + \sin^3(\beta_s - \phi)]} \times \frac{\left[\dfrac{\tan\phi}{\tan(\beta_d - \phi)} - 1\right]^2}{\left[1 - \dfrac{\tan\phi}{\tan(\beta_d - \phi)}\right]^{3/2}} \right\}^{1/3}. \quad (9)$$

For the highly-wetting liquids, of primary interest in the present study, the contact angles and cavity cone angles, as well as the differences between these two values, are very small. For small dynamic contact angles, it is possible to approximate the trigonometric relations as

$$\tan\phi \approx \phi; \quad \tan(\beta_d - \phi) \approx \beta_d - \phi;$$
$$\sin(\beta_d - \phi) \approx \beta_d - \phi; \quad \cos(\beta_s - \phi) \approx 1. \quad (10)$$

Hence, for small dynamic contact angles equation (9) can be simplified to

$$\frac{R_1}{R_0} \cong \frac{\left(1 - \dfrac{2\phi}{\beta_d}\right)^{1/2}}{\{1 + \phi[2 - 3(\beta_s - \phi) + (\beta_s - \phi)^3]\}^{1/3}} = f(\beta_s, \beta_d, \phi). \quad (11)$$

The comparison of equations (9) and (11) for a small contact angle, say $\beta_s = 2°$, has shown that for the small β_d cases, little difference between the two models is observed; but for the large β_d cases, the two curves diverge slightly (Fig. 9). When $\beta_d - \beta_s = 60°$, equation (11) deviates by just 8.4% (maximum) from equation (9), even though the small dynamic contact angle approximations do not apply under such conditions. This indicates that equation (11) is valid for all highly-wetting liquids even when dynamic contact angles are large. While the radius ratio, R_1/R_0, increases with β_d, Fig. 9 shows that this ratio remains less than unity. This result reveals that for highly-wetting liquids, bubbles at critical radii always occur inside the cavities, regardless of β_d values.

It is important to recall that the larger the interface velocity, the larger the dynamic contact angle and, thus, the larger the trapped vapor/gas volume and bubble embryo radius. Consequently, the incipience superheat can be expected to vary with the liquid/gas interface velocity. For high interface velocities, the required superheat for incipience may lie substantially below the values for a quiescent pool.

INFLUENCE OF CONTACT ANGLE HYSTERESIS ON THE BUBBLE GROWTH PROCESS

The formation (trapping) of a vapor/gas embryo in a surface cavity creates a void into which superheated liquid can evaporate. This evaporation increases the volume of the gaseous mixture and continues until the bubble reaches equilibrium conditions. This behavior and the change of the bubble radius through the four distinct stages of bubble growth (see Figs. 3 and 4), will be examined in the following.

1. *Contact angle readjustment* (*Fig.* 4(*a*))

Following the filling of the cavity by liquid (representing the first stage of the bubble growth process), a small increase in bubble volume and the resulting motion of the vapor/liquid interface due to contact angle hysteresis, will lead to a decrease in contact angle to its static (liquid) receding value, $\beta_{s,R}$. During this process, the bubble three-phase line remains fixed at its initial position on the cavity wall. With radius R_2 corresponding to $\beta_{s,R}$ and R_1 corresponding to β_s, the following geometric relationship can be determined:

$$\frac{R_2}{R_1} = \frac{\cos(\beta_s - \phi)}{\cos(\beta_{s,R} - \phi)}. \quad (12)$$

For perfectly smooth and homogeneous surfaces,

$\beta_{s,R} = \beta_s$ and $R_2 = R_1$. However, for real surfaces $\beta_{s,R}$ is always less than β_s [11]. Therefore, $R_2 < R_1$ and this contact angle readjustment will result in an increase in the inverse bubble radius (stage 1 of Fig. 3). For highly-wetting liquids, the static receding contact angle, $\beta_{s,R}$, and the static equilibrium contact angle, β_s, are small; thus, $R_2 \approx R_1$. The resulting increase in incipience superheat is expected to be negligible in these cases (i.e. stage 1 (Fig. 3) readjustment is unimportant).

The change in bubble embryo volume during this contact angle readjustment is

$$\Delta V = \pi R_1^3 \frac{\cos(\beta_s - \phi)}{\cos(\beta_{s,R} - \phi)} \times \left\{ \left[1 - \sin(\beta_s - \phi) + \frac{\sin(\beta_s - \beta_{s,R})}{\cos(\beta_{s,R} - \phi)} \right]^2 - \frac{1}{3}\left[1 - \sin(\beta_s - \phi) + \frac{\sin(\beta_s - \beta_{s,R})}{\cos(\beta_{s,R} - \phi)} \right]^3 - \frac{1}{3}[1 - \cos(\beta_s - \phi)]^2[2 + \cos(\beta_s - \phi)] \right\}. \quad (13)$$

Since both the inverse bubble radius and the bubble volume increase during this process, $\Delta(1/R)/\Delta V$ is positive and the bubble growth is restrained (positive-sloped segment in the coordinates of Fig. 3). Following Thormählen [24], this process will, henceforth, be referred to as 'stable bubble growth'.

2. *In-cavity growth (Fig. 4(b))*

As additional vapor forms and the embryonic bubble grows, the liquid/vapor interface moves toward the mouth of the cavity. At the beginning of this phase, the contact angle, β, changes immediately and spontaneously from its static receding value, $\beta_{s,R}$, to a dynamic contact angle value, β_d, where $\beta_s \geq \beta_d \geq \beta_{d,R}$. It remains at its dynamic value throughout this process. The bubble radius during this phase can be calculated as

$$R = \left\{ \frac{1}{\pi} \frac{3V}{\dfrac{\cos^3(\beta_d - \phi)}{\tan\phi} + [2 - 3\sin(\beta_d - \phi) + \sin^3(\beta_d - \phi)]} \right\}^{1/3}. \quad (14)$$

This is equation (7) with V substituted for V_g and β_d for β_s. It describes the bubble behavior at stage 2 in Fig. 3. The slope of the segment corresponding to this process is negative. Therefore, the bubble will continuously expand until it reaches the edge of the cavity.

3. *Growth at the cavity mouth (Fig. 4(c))*

As the bubble moves towards the mouth of the cavity, the contact angle retains the appropriate dynamic value. However, at the mouth, the contact angle readjusts to its static receding value and the bubble radius changes correspondingly from R_3 to R_4. Two ranges can be distinguished in this phase.

(a) Range where the center of the curvature of the bubble interface moves from point 0_3 to A.

The radius, R, decreases continuously from R_3 to R_0 (the minimum value of radius for this stage) while the volume of the bubble increases. Consequently, the slope of this subsegment in the coordinates of Fig. 3 is positive and the growth is stable. The radius R_3 is

$$R_3 = \frac{R_0}{\cos(\beta_d - \phi)} \quad (15)$$

and, clearly

$$R_3 > R_2. \quad (16)$$

(b) Range where the center of the curvature of the bubble moves from point A to 0_4 (corresponding to $\beta = \beta_{s,R}$, $R = R_4$).

The bubble radius continues to increase with increasing volume. The slope of the subsegment in Fig. 3 is negative and the bubble grows without restraint until it leaves the heated surface

$$R_4 = \frac{R_0}{\sin(\beta_{s,R})} \quad (17)$$

and

$$R_4 > R_0. \quad (18)$$

4. *Growth on the outer surface and bubble departure*

After reaching the point $R = R_4$, the bubble will continuously expand until it leaves the heated surface. This process can be described as a 'bubble snapping process' (Fig. 10). As discussed by Shakir and Thome [30], this is a complex process controlled by the dynamic departure of the bubble from the surface. This process determines the radius of the trapped vapor embryo under a departing bubble and, consequently, influences the generation of subsequent bubbles from the same site.

Figure 10 illustrates the bubble snapping process over a conical cavity on a flat plate. In the first stage, the contact angle of the bubble interface maintains its static receding value as the bubble expands on the heated surface (Fig. 10(a)). Along with the increase of the bubble volume, the bubble elongates due to the increase of the buoyancy force (Fig. 10(b)). This process continues until the static advancing contact angle is reached and the bubble neck is formed (Fig. 10(c)). Figure 10(d) assumes that the three-phase boundary line moves inside the cavity while the neck area of the bubble rapidly contracts.The neck finally vanishes as the bubble snaps, then departs from the surface. The vapor/air left in the cavity becomes the embryo of the subsequent bubble (Fig. 10(e)).

As discussed in a previous section, the radius of a bubble embryo is proportional to the volume of the

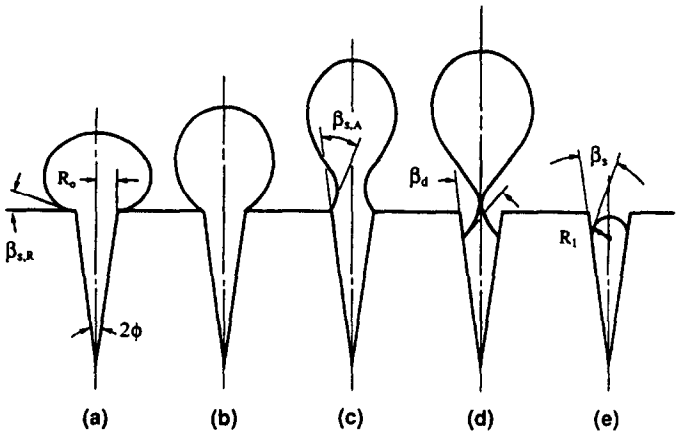

FIG. 10. Bubble 'snapping' process.

trapped vapor/gas and, thus, is also proportional to the dynamic contact angle. Since the superheat required for boiling incipience varies inversely with the bubble radius, it can be concluded that for large values of β_d the incipience superheat decreases. In the pool boiling of highly-wetting liquids the microscale velocity field, produced by a departing bubble, can be expected to result in a larger dynamic contact angle than initially experienced by an active nucleation site. Consequently, in keeping with empirical observations [30], the superheat required to sustain nucleate boiling may well fall below the initial incipience superheat and vary substantially with the details of the bubble-pumped velocity field adjacent to the heated surface. In situations where the initial dynamic contact angles may already be relatively large, this effect may be far weaker and produce only modest, or negligible, drop in wall superheat.

CRITICAL BUBBLE RADIUS AND INCIPIENCE SUPERHEAT

Critical radius of the embryonic bubble

The minimum radius of the bubble nucleus, called the critical radius, is an important factor in nucleate boiling since it determines the superheat $(\Delta T_s)_i$ required to initiate nucleate boiling.

In previous sections it was shown that for highly-wetting liquids the critical bubble radius is usually less than the cavity radius and incipience occurs inside the cavity.

The criterion for determining whether the critical radius is within the cavity or at the mouth of the cavity for liquids with moderate contact angles but with $\beta_s < \pi/2$, is found by combining equations (8), or (9), and (12)

$$\frac{R_2}{R_0} = \frac{\cos(\beta_s - \phi)}{\cos(\beta_{s,R} - \phi)} F(\beta_s, \beta_d, \phi)$$
$$= G(\beta_s, \beta_d, \beta_{s,R}, \phi). \quad (19)$$

When $G > 1$, the critical radius is at the mouth of the cavity. When $G < 1$ the critical conditions have been met and the bubble grows spontaneously within the cavity; thus, the geometry at the mouth of the cavity is unimportant.

For poorly-wetting liquids with contact angles $\pi/2 \leqslant \beta_s < \phi + \pi/2$, the important radii are R_2 and R_4. The ratio of the two candidates for minimum radius during bubble growth is given by

$$\frac{R_2}{R_4} = F(\beta_s, \beta_d, \phi) \sin \beta_{s,R}$$
$$= H(\beta_s, \beta_d, \beta_{s,R}, \phi). \quad (20)$$

The critical radius, R_C, is $\min\{R_2, R_4\}$.

Heterogeneous incipience superheat

Following the classical analysis of nucleate boiling [25], a force balance on the liquid/vapor interface, assumed to be a uniform curvature surface, can be used to determine the incipience vapor pressure, as

$$P_v^* - P_\ell = \frac{2\sigma}{R_C} - \Sigma P_g^* \quad (21)$$

where P_ℓ is the equilibrium liquid pressure over the bubble interface and R_C the critical radius. The superscript '*' indicates a pressure inside the bubble. The ΣP_g^* term contains the partial pressures of different gases within the bubble. As discussed in ref. [31], for high-solubility fluids such as Fluorinerts and Freons, dissolved gas may play a very important role in nucleate boiling. The saturation temperature at the vapor pressure, P_v, can be determined as [32]

$$T_s = \frac{b}{a - \ln(P_v)} \quad (22)$$

where a and b are empirical constants. If T is in kelvin and P is in N m^{-2}, $a = 22.3329$ and $b = 3566.68$ for FC-72 (correlated from 3M FC-72 data). For highly-wetting liquids the bubble nuclei are very small and are inside the cavities. Therefore, the bubble temperature can be taken to equal the wall temperature, T_w, so that both the vapor pressure, P_v, and the surface tension, σ, can be evaluated at the wall temperature. For non-

polar fluids, or fluids with low dipole moments, surface tension varies with the temperature as [33]

$$\sigma = \sigma_0 \left(1 - \frac{T_w}{T_c}\right)^{\mu} \tag{23}$$

where T_C is the critical temperature and $\sigma_0 = 0.042705$ N m^{-1}, $\mu = 1.2532$ for FC-72 (this fit is based on a combination of the data from McLure *et al.* [34] for $T < 340$ K and Skripov and Firsov [35] for $T > 340$ K). Also, for saturated conditions, the vapor pressure can be expressed as

$$P_v^* = \exp\left(a - \frac{b}{T_w}\right). \tag{24}$$

The governing equation (21) can be re-expressed as

$$\exp\left(a - \frac{b}{T_w}\right) - P_\ell = \frac{2\sigma(T_w)}{R_0 f(\beta_s, \beta_d, \phi)} - \Sigma P_g^* \tag{25}$$

where $f(\beta_s, \beta_d, \phi)$ is found from equation (11). Since this equation is a transcendental equation in the dependent variable, T_w, it must be solved by a trial and error method.

A frequently-used model employs the Clausius–Clapeyron relation [25] (instead of equations (22) and (24)) and bases the surface tension on the saturation temperature. A comparison of superheats calculated from the present model (equation (25)) and this frequently-used model of a highly-wetting liquid for $\beta_s = 2°$ and $R_0 = 0.5$ μm, is given in Fig. 11 for a system free of non-condensable gas. From this figure it may be seen that the model which utilizes the Clausius–Clapeyron relation deviates from the present model for all dynamic contact angles. Thus, though the frequently-used model is simpler than equation (25), the present model is recommended since: (a) the assumption of linearity of the saturation curve, as must be done to use the Clausius–Clapeyron relation, may be improper for situations of large superheat with highly-wetting liquids and (b), since the position of the critical radius is always inside of the cavity for highly-wetting liquids, the surface tension at the bubble interface should be evaluated at the wall temperature rather than at the saturation temperature.

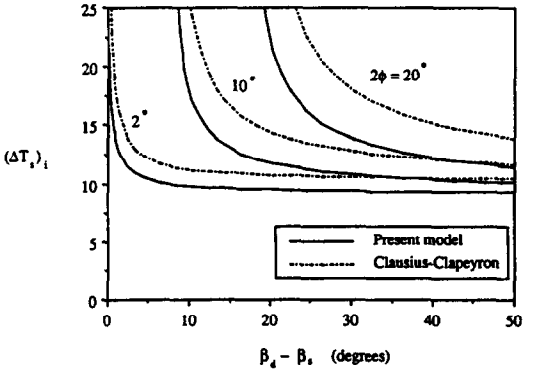

FIG. 11. Comparison of the present model and the frequently-used model employing the Clausius–Clapeyron relation for boiling incipience superheat of highly-wetting liquids ($\beta_s = 2°$ and $R_0 = 0.5$ μm).

Figure 11 also reveals that $(\Delta T_s)_i$ can be greatly reduced by increasing dynamic contact angles at the range where β_d approaches the cavity angle.

CONCLUSIONS

The preceding has explored the phenomena associated with the incipience of boiling via heterogeneous nucleation in highly-wetting liquids. A detailed analysis of the contact angle effects on vapor/gas trapping and the bubble growth processes, has yielded analytic relations for the heterogeneous incipience superheat.

In agreement with previous investigators, the critical radius for highly-wetting liquids has been shown, in all cases, to lie below the mouth radius of the active cavity. For moderately-wetting liquids, the critical radius can be determined by the two derived criteria (equations (19) and (20)).

The study has shown how changes in the dynamic contact angle can change the trapped volume of vapor/gas, which constitutes the bubble embryo. The dynamic contact angle, which is dependent on the velocity of the three-phase contact line, is always greater than the static equilibrium contact angle. Consequently, at high interface velocities, the dynamic contact angle, for highly-wetting liquids, may be sufficiently large to trap gas and form bubble embryos in larger surface cavities. Since the incipience superheat depends on the radius of curvature of the embryonic bubble, it must depend on the trapping interface velocity and filling conditions. The study thus shows that the incipience superheat can be far lower than previously thought due to the difference between the dynamic and static contact angles. Furthermore, for highly-wetting liquids, variations in contact angle during bubble embryo formation and bubble growth, induced by changes in the direction and magnitude of the liquid/vapor interface velocity, can substantially influence the incipience superheat and may well explain the wide variations previously reported in this quantity.

Based on the analysis of the bubble trapping process, a new model (modified Lorenz model), which involves both the static and dynamic contact angle, is proposed to calculate the ratio of the embryonic bubble radius to the cavity radius. For highly-wetting liquids this model can be expressed in a very simple form. The proposed model is based on the formation in a surface cavity of a vapor/gas embryo into which superheated liquid can evaporate. It is important to note that the use of this new model, or Lorenz's model, for evaluating incipience superheat requires that no diffusion of gas or condensation of vapor transpire between the trapping and incipience processes.

Theoretical analysis also shows that static contact angle hysteresis can influence the bubble growth process for moderately-wetting liquids. For highly-wetting liquids, this effect is expected to be small.

Acknowledgements—The authors are grateful to the Commercial Chemicals Division of the 3M Company for supporting this work.

REFERENCES

1. R. M. Burger, R. K. Cavin III, W. C. Holton and L. W. Sumney, The impact of ICs on computer technology, *IEEE Comput.* 88–95 (October 1984).
2. A. Bar-Cohen, Future opportunities and challenges in heat transfer—an industrial perspective, *Heat Transfer Engng* 7, 82–88 (1986).
3. C. Corty and A. S. Foust, Surface variables in nucleate boiling, *Chem. Engng Prog. Symp. Ser., A.I.Ch.E.* **51**, 1–12 (1955).
4. S. G. Bankoff, Entrapment of gas in the spreading of a liquid over a rough surface, *A.I.Ch.E. Jl* **4**, 24–26 (1958).
5. P. Griffith and J. D. Wallis, The role of surface conditions in nucleate boiling, *Chem. Engng Prog. Symp. Ser., A.I.Ch.E.* **56**, 49–63 (1960).
6. Y. Y. Hsu, On the size range of active nucleation cavities on a heating surface, *J. Heat Transfer* **84**, 207–216 (1962).
7. J. J. Lorenz, The effects of surface conditions of boiling characteristics, Ph.D. thesis, Massachusetts Institute of Technology, Cambridge, Massachusetts (1972).
8. R. Cole, Boiling nucleation. In *Advances in Heat Transfer*, Vol. 10, pp. 86–166. Academic Press, New York (1974).
9. Ramé-hart Inc., Surface Science Instrumentation, Products Catalog, Mountain Lakes, New Jersey (1985).
10. A. M. Schwartz and S. B. Tejada, Studies of dynamic contact angle on solids, *J. Colloid Interface Sci.* **38**, 359–375 (1972).
11. R. E. Johnson, Jr. and R. H. Dettre, Wettability and contact angles. In *Surface and Colloid Science* (Edited by E. Matijević), Vol. 2, pp. 85–153. Wiley-Interscience, New York (1969).
12. A. E. Bergles, N. Bakhru and J. W. Shires, Jr., Cooling of high-power-density computer components, M.I.T., Engineering Projects Laboratory Report No. DSR 70712-60, Cambridge, Massachusetts (1968).
13. S. P. Liaw and V. K. Dhir, Effect of surface wettability on transition boiling heat transfer from a vertical surface, *Proc. 8th Int. Heat Transfer Conf.*, Vol. 4, pp. 2031–2036 (1986).
14. R. L. Webb, Nucleate boiling on porous coated surface, ASME Paper 83-HT-37 (1983).
15. R. D. Danielson, L. Tousignant and A. Bar-Cohen, Saturated pool boiling characteristics of commercially available perfluorinated inert liquids, 2nd ASME/JSME Thermal Engng Joint Conf., Hawaii, Vol. 3, pp. 419–430 (1987).
16. W. J. Marsh and I. Mudawwar, Effect of surface tension and contact angle on sensible heating and boiling incipience in dielectric falling films, HTD-Vol. 96, *Proc. Nat. Heat Transfer Conf.*, Vol. 1, pp. 543–550 (1988).
17. J. G. Truong, Ellipsometric and interferometric studies of thin liquid films wetting on isothermal and non-isothermal surfaces, Ph.D. thesis, Rensselaer Polytechnic Institute, Troy, New York (1987).
18. 3M Company, Product Manual, FLUORINERT® Electronic Liquids, St. Paul, Minnesota (1987).
19. R. E. Johnson, Jr. and R. H. Dettre, Dynamic contact angles and contact angle hysteresis, *J. Colloid Interface Sci.* **62**, 205–212 (1977).
20. J. Chappuis, Contact angle. In *Multiphase Science and Technology* (Edited by G. F. Hewitt, J. M. Delhaye and N. Zuber), pp. 387–505. Hemisphere/McGraw-Hill, New York (1982).
21. J. R. Howell and R. Siegel, Incipience, growth, and detachment of boiling bubble on saturated water from artificial nucleation sites of known geometry and size, *Proc. 3rd Int. Heat Transfer Conf.*, Vol. 4, pp. 12–23 (1966).
22. C. Y. Han and P. Griffith, The mechanism of heat transfer in nucleate pool boiling—I. Bubble initiation, growth and departure, *Int. J. Heat Mass Transfer* **8**, 887–904 (1965).
23. K. Mizukami, The effect of gases on the stability and nucleation of vapor bubble nuclei, *Lett. Heat Mass Transfer* **4**, 17–24 (1977).
24. I. Thormählen, Superheating of liquids at the onset of boiling, *Proc. 8th Int. Heat Transfer Conf.*, Vol. 4, pp. 2001–2006 (1986).
25. W. M. Rohsenow, J. P. Hartnett and E. G. Ganić, *Handbook of Heat Transfer Fundamentals* (2nd Edn), Chap. 12. McGraw-Hill, New York (1985).
26. W. Porteous and M. Blander, Limits of superheat and explosive boiling of light hydrocarbons, halocarbons, and hydrocarbon mixtures, *A.I.Ch.E. Jl* **21**, 560–566 (1975).
27. M. Blander and J. L. Katz, Bubble nucleation in liquids, *A.I.Ch.E. Jl* **21**, 833–848 (1975).
28. C. T. Avedisian, The homogeneous nucleation limits of liquids, *J. Phys. Chem. Ref. Data* **14**, 695–729 (1985).
29. A. Bar-Cohen and T. W. Simon, Wall superheat excursions in the boiling incipience of dielectric fluids, *Heat Transfer Engng* **9**, 19–31 (1988).
30. S. Shakir and J. R. Thome, Boiling nucleation of mixtures on smooth and enhanced surfaces, *Proc. 8th Int. Heat Transfer Conf.*, Vol. 4, pp. 2081–2086 (1986).
31. W. Tong, T. W. Simon and A. Bar-Cohen, Effect of dissolved gas on boiling incipience in highly-wetting liquids, *Proc. 5th Miami Int. Symp. on Multiphase Transport and Particulate Phenomena*, Miami. Hemisphere, Washington, DC (1989).
32. R. C. Reid, J. M. Prausnitz and B. E. Poling, *The Properties of Gases and Liquids* (4th Edn). McGraw-Hill, New York (1987).
33. S. D. van der Waals, Thermodynamische theorie der kapillarität unter voraussetzung stetiger dichteänderung, *Z. Phys. Chem.* **13**, 657–725 (1894).
34. I. A. McLure, A. M. S. Virgilio and B. Edmonds, Surface tension of perfluoropropane, perfuoro-butane, perfluoro-n-hexane, perfluoro-octane, perfluorotributylamine and n-pentane, *J. Chem. Soc., Faraday Trans.* **78**, 2251–2257 (1982).
35. V. P. Skripov and V. V. Firsov, Surface tension of perfluoroalkanes, *Russian J. Phys. Chem.* **42**, 653–656 (1968).
36. K. Watanabe and M. Okada, Surface tension of several halogenated hydrocarbons, *Proc. 7th Symp. on Thermophysical Properties*, pp. 851–863 (1977).

APPENDIX: CALCULATIONS OF THE WALL TEMPERATURE AND THE WALL SUPERHEAT

This is a numerical example to show how to calculate the wall temperature using equation (25). Choosing R-113 as the working liquid, the contact angle values are estimated as

$$\beta_s = 2^\circ, \quad \beta_d = 20^\circ.$$

Assume the cavity geometry can be described by

$$R_0 = 0.5\ \mu\text{m}, \quad 2\phi = 12^\circ.$$

Using equation (11), the critical bubble radius, R_c, is found to be 0.30 μm.

The surface tension of R-113 is given as [36]

$$\sigma = 0.055610\left(1-\frac{T}{487.25}\right)^{1.2384}$$

and the coefficients a and b in equation (24) are [31]

$$a = 21.8400, \quad b = 3303.70.$$

Assuming that there is no dissolved gas in the liquid and the system is under the atmospheric pressure, thus, equation (25) can be written as

$$\exp\left(21.8400-\frac{3303.70}{T_w}\right)-101\,325$$

$$=370\,733\left(1-\frac{T_w}{487.25}\right)^{1.2384}$$

The wall temperature calculated from the above equation is 340.2 K. Since the saturation temperature of R-113 is 320.2 K at 1 atm pressure, the wall superheat is 20 K.

EFFET DE L'ANGLE DE CONTACT SUR LA NAISSANCE DE L'EBULLITION DANS DES LIQUIDES FORTEMENT MOUILLANTS

Résumé—La difficulté dans la prédiction de la naissance de l'ébullition dans des liquides fortement mouillants a ralenti l'application du refroidissement par immersion dans l'industrie électronique. On éclaire ici ce phénomène en examinant l'influence de l'angle de contact solide/liquide et l'hystérésis de l'angle de contact sur la naissance de la surchauffe. Les résultats suggèrent que des variations de l'angle de contact, induites par des changements de direction et de grandeur de la vitesse de l'interface liquide/vapeur, peut sensiblement affecter la formation des embryons de bulle et peut bien expliquer la grande dispersion expérimentale dans les valeurs du début de surchauffe reportées pour des liquides fortement mouillants.

EINFLUSS DES RANDWINKELS AUF DEN SIEDEBEGINN VON GUT BENETZENDEN FLÜSSIGKEITEN

Zusammenfassung—Der Siedebeginn von gut benetzenden Flüssigkeiten ist schwer vorherzusagen ; dadurch wurde die Anwendung der Tauchkühltechnik in der Elektronik-Industrie verzögert. Durch die Untersuchung des Einflusses des dynamischen Randwinkels zwischen dem festen Körper und der Flüssigkeit und der Hysterese des Randwinkels auf die Überhitzung beim Siedebeginn wird neue Einsicht in dieses Phänomen gewonnen. Die Ergebnisse weisen darauf hin, daß die Variation des Randwinkels, die von der Änderung der Richtung und der Größe der Geschwindigkeit der Flüssigkeit–Dampf-Phasengrenze verursacht wird, die Entstehung des Blasenkeims wesentlich beeinflussen kann. Das kann die große Streuung der gemessenen Überhitzung beim Siedebeginn von gut benetzenden Flüssigkeiten gut erklären.

ВЛИЯНИЕ КРАЕВОГО УГЛА СМАЧИВАНИЯ НА ВОЗНИКНОВЕНИЕ КИПЕНИЯ ВЫСОКОСМАЧИВАЮЩИХ ЖИДКОСТЕЙ

Аннотация—Трудность определения возникновения кипения высокосмачивающих жидкостей препятствовала использованию в электронной промышленности способа охлаждения погружением. Предпринята новая попытка объяснить эти явления на основе исследования влияния динамического краевого угла между твердым телом и жидкостью, а также гистерезиса этого угла на возникновение перегрева. Результаты позволяют предположить, что варьирование краевого угла, вызванное изменениями направления и величины скорости движения границы раздела жидкости и пара, может оказывать существенное влияние на зарождение пузырьков и позволяет объяснить широкий разброс экспериментальных значений возникновения перегрева для высокосмачивающих жидкостей.